Magnetic Diagnostics for Wendelstein 7-X during the first Operation Phase

K. Rahbarnia[1], A. Cardella[2], M. Endler[1], D. Hathiramani[1], J. Geiger[1], O. Grulke[1], T. Klinger[1], U. Neuner[1], T. Sunn Pedersen[1], A. Werner[1], T. Windisch[1]

[1] *Max-Planck Institute for Plasma Physics, Wendelsteinstr. 1, 17489 Greifswald, Germany*

[2] *Former W7-X, presently JT-60SA project, F4E c/o IPP Boltzmannstr. 2, 85748 Garching, Germany*

During the first operation phase of the stellarator Wendelstein 7-X various magnetic diagnostic systems will be commissioned with respect to optimization of data acquisition and data evaluation. It is essential to obtain detailed information about key quantities like the plasma energy and plasma currents by measuring the magnetic flux. A reconstruction of the plasma equilibrium for different scenarios will allow to investigate and compare theoretical optimization criteria for W7-X, e.g. the reduction of Bootstrap and Pfirsch-Schlüter currents. Measurements of plasma current distributions are necessary to derive plasma pressure anisotropies and contribute to energy and particle confinement studies. Information on direction and strength of localized current filaments and derived magnetic island formations will be used in divertor control systems.

A common Ansatz for the interpretation of magnetic flux measurements is [1]

$$2\frac{\Delta\Phi}{\Phi_t} = \frac{(B_p)^2}{(B_t)^2} - \beta\,, \tag{1}$$

with the toroidal magnetic flux Φ_t, the change of the flux due to the plasma pressure $\Delta\Phi$, the toroidal and poloidal magnetic fields B_t and B_p and the ratio between the volume averaged plasma pressure p to the magnetic field pressure $\beta = 2\mu_0 p/B^2$. Basically the contributions to the measured flux signal $\Delta\Phi$ can be expressed as [2]

$$\Delta\Phi = \Delta\Phi_{dia} + \Delta\Phi_{Ip} + \Delta\Phi_{ext} + \Delta\Phi_{vac}\,. \tag{2}$$

Hence to obtain the plasma energy, which is directly related to the diamagnetic flux $\Delta\Phi_{dia}$, the flux change due to the net plasma current $\Delta\Phi_{Ip}$ and due to eddy currents in the external coils and vessel structures has to be considered. The flux related to the vacuum magnetic configuration is described by the last term in Eq. (2) $\Delta\Phi_{vac}$.

The proper determination of the plasma equilibria for the strongly 3D-shaped plasmas in W7-X is only accurate enough by using numerical methods (e.g. VMEC [3]). The plasma energy, Pfirsch-Schlüter currents, plasma currents and current distributions are measured by diamagnetic loops, saddle loops and Rogowski coils. A high steady state heat load up to several

$100\,\mathrm{kW/m^2}$ lead to a sophisticated thermal shielding and actively cooled structural design to ensure that during operation the temperature of critical diagnostic components do not exceed the specified maximal values. Technical details of these diagnostics due to the skewed three-dimensional shape of the plasma vessel and restricted boundary conditions will not be discussed in this context. One of the main challenges specifically during the long pulse operation of W7-X up to 1800 s are low signal amplitudes and the long integration times. In Tab. 1 an overview of the expected magnetic flux signals related to the total plasma current, Pfirsch-Schlüter currents and the plasma energy accumulated based on different discharge scenarios is presented.

	total plasma current	Pfirsch-Schlüter current	plasma energy
expected value / accuracy	< 200 kA / 100 A	∼ 50 kA / 100 A	1–5 MJ / 10 kJ
magnetic flux	63 mWb / 30 μWb	60 mWb / 34 μWb	50 mWb / 10 μWb
signal amplitude	15–80 V	4–15 V	30–570 V
required accuracy	1–35 nV	110–330 nV	∼ 1 μV
diagnostic	Rogowski coils	Saddle loops	Diamagnetic loops

Table 1: *Overview of expected magnetic flux signals and corresponding equilibrium diagnostics*

In order to study magnetic fluctuations, e.g. due to stellarator specific Alfvén eigenmode activity, W7-X possesses an arrangement of 125 calibrated Mirnov coils mounted behind wall protection panels inside the vacuum vessel. They are installed in 4 poloidal arrangements (3 closed, 1 open) and a number of toroidally distributed probes. For future operation phases the set will be completed by 42 additional probes mounted on the wall panels directly. Tab. 2 shows expected magnetic fluctuation levels

expected fluctuation level $\tilde{b}/B_0$	$10^{-5} - 10^{-3}$
magnetic field change	$8\,\mu\mathrm{T} - 3\,\mathrm{mT}$
induced voltage	$5\,\mathrm{mV} - 1.1\,\mathrm{V}$
required accuracy	$\sim 1\,\mathrm{mV}$
frequency range	$10^3 - 10^6\,\mathrm{Hz}$

Table 2: *Expected magnetic fluctuations amplitudes, required accuracy and dynamic range for the installed Mirnov coils*

Each Mirnov coil is frequency and phase calibrated in an ex-vessel test-stand including main and stray components. The calibration results for the main component (Y-direction) is shown in Fig. 1. The measurements in Fig. 1(a) and (c) are normalized to the amplitude and phase of a differential loop, which was previously used to calibrate the test-stand. The calibration measurement of the Mirnov coil is done for two 180° flipped orientations (red and blue lines in Fig. 1). They agree well for frequencies $10^3 - 10^6$ Hz (Fig. 1(b), difference between both orientations <1%).

The phase deviation (Fig. 1(c)) for high frequencies can be attributed to the self-inductance of the probe. At low frequencies the phase differs due to the used implemented FFT analysis software of the test-stand.

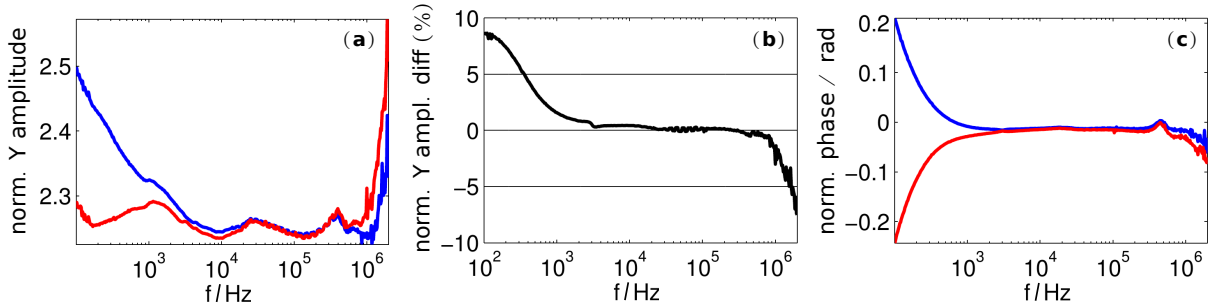

Figure 1: *Mirnov coil calibration on a test-stand, (a) Normalized amplitude in Y-direction for two* 180° *flipped orientations (red and blue lines), (b) difference of both orientations, (c) normalized phase in Y-direction*

To account for geometrical asymmetries of the Mirnov coil, misalignment within the test-stand and capacitive as well as inductive pickup, the stray components (X-, and Z-direction) are also measured by a corresponding alignment of the coil in the test-stand (Fig. 2). The relative amplitude of the stray components in X-, and Z-direction is in the order of 5% with respect to the main Y-component for both orientations.

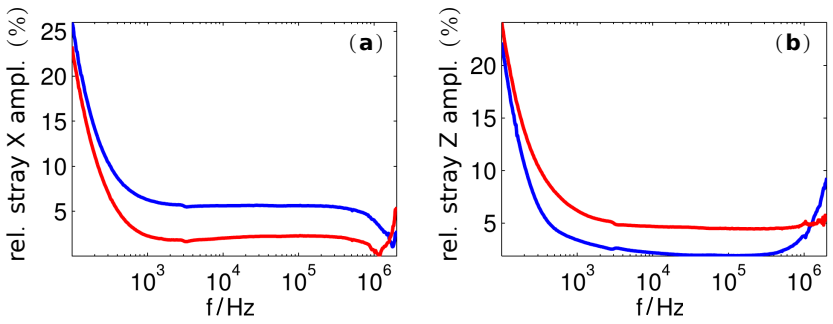

Figure 2: *Relative amplitude of the stray components in X-direction (a) and Z-direction (b) with respect to the main Y-component for two* 180° *flipped orientations (red and blue lines)*

A possible mode analysis scheme similar to the method previously used at W7-AS will be as follows. After a proper mapping of the Mirnov coil positions to magnetic coordinates, time resolved frequency spectra can be calculated by applying Wavelet analysis techniques. Deriving corresponding Lomb periodograms provide toroidal and poloidal mode number spectra. Assuming appropriate plasma density profiles the magnetic equilibrium for a certain operation scenario is reconstructed by using numerical methods (e.g. VMEC). Based on the equilibrium the Alfvén continuum for this configuration is obtained from continua codes like CONTI [4]. Altogether by carefully analysing the expected gap structure within the Alfvén continuum and comparisons

with the measurements, the actual mode structure can be identified.

An example Alfvén continuum (lower frequency part) as calculated by CONTI using all information available from the VMEC code for a configuration of W7-X obtained from Ref. [5] is depicted in Fig. 3 [6]. The frequency ω normalized to the relevant Alfvén frequency ω_A is shown as a function of the flux label $s \in [0,1]$, which corresponds to the normalized toroidal magnetic flux using Boozer coordinates. The branches forming the helicity-induced Alfvén eigenmodes (HAE) and the toroidal Alfvén eigenmodes (TAE) gaps have been especially highlighted using different colours. For this particular case measured modes structures would most likely be related to these gaps.

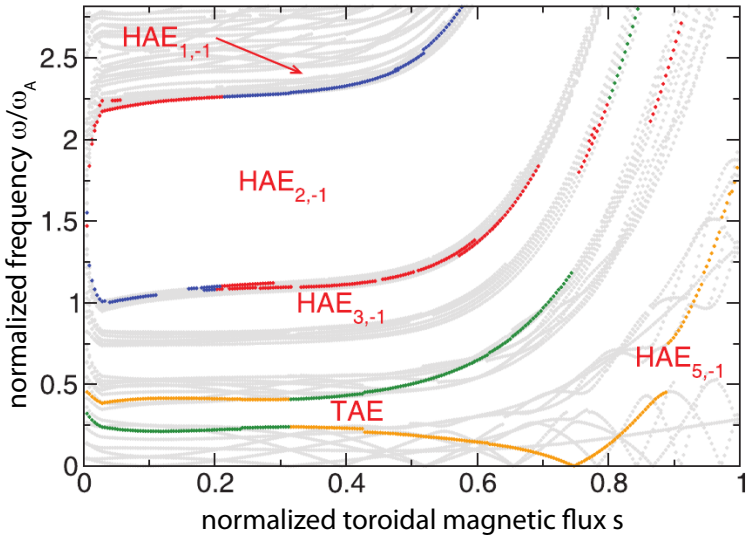

Figure 3: *Example Alfvén continuum for a certain configuration of W7-X calculated with CONTI [6]*

This project has received funding from the Euratom research and training programme 2014-2018.

References

[1] S.I. Braginskii and V.D. Shafranov, Plasma Physics and Problem of Controlled Thermonuclear Reactions vol 2, Oxford: Pergamon, p. 39 (1959)

[2] T. Yamaguchi et al., Plasma Phys. Control. Fusion **48**, L73-L85 (2006)

[3] S. P. Hirshman, W. I. van Rij, and P. Merkel, Comput. Phys. Commun. **43**, 143 (1986)

[4] A. Könies and D. Eremin, Phys. Plasmas **17**, 012107 (2010)

[5] M. Drevlak, D. Monticello, and A. Reiman, Nucl. Fusion **45**, 731 (2005)

[6] A. Könies and R. Kleiber, Phys. Plasmas **19**, 122111 (2012)